Article ID: 1000-324X(2019)12-1334-07 **DOI:** 10.15541/jim20190057

Preparation of CeO_2/Flake-like CdS Composites as High-performance Photoanodes for Photoelectrochemical Cathodic Protection

WEI Ke-Nian[1,2], LIU Zhan[2], ZUO Shi-Xiang[2], YAN Xiang-Yu[2], WU Feng-Qin[2], LI Xia-Zhang[2], YAO Chao[1,2], LIU Xiao-Heng[1]

(1. Key Laboratory for Soft Chemistry and Functional Materials, Ministry of Education, Nanjing University of Science and Technology, Nanjing 210094, China; 2. Advanced Catalysis and Green Manufacturing Collaborative Innovation Center, School of Petrochemical Engineering, Changzhou University, Changzhou 213164, China)

Abstract: CeO_2/CdS nanocomposites with the function of storing electrons and physical barrier were fabricated for photocathodic protection through a stepwise synthetic route. The obtained smples were characterized by XRD, TEM, UV-Vis and PL. The photoelectrochemical properties of CeO_2/CdS with different mass ratios were investigated under white light irradiation. The maximum photocurrent density of CeO_2/CdS (mass ratio 0.2∶1.0) is 700 μA·cm^{-2} and the potential of the 304 stainless steel coated with CeO_2/CdS (mass ratio 0.2∶1.0) shifts to –650 mV (*vs.* SCE), which is significantly lower than the corrosion potential (–200 mV *vs.* SCE). The above results indicate that the CeO_2/CdS composites exhibit remarkable photo cathodic properties which are attributed to the heterostructure of CeO_2 nanoparticles and CdS nanosheets, and the structure facilitates the separation of photo-induced electron and hole. Furthermore, the CeO_2/CdS composites can also provide cathodic protection for 12 h in the dark.

Key words: CeO_2/CdS composite; heterostructure; physical barrier; photoelectrochemical cathodic protection

Steels have been widely used in marine engineering such as ship hulls, boilers and subsea equipment. However, steel corrosion has been getting more and more attention. Photoelectrochemical (PEC) cathodic protection is considered as an eco-friendly method for metals anticorrosion. The n-type semiconductor photoanode provides the photo-generated electrons for metals to achieve cathodic protection. At present, the semiconductors used for photocathode protection are mainly TiO_2, $SrTiO_3$ and ZnO[1]. However, the semiconductors with a wide band gap (E_g) only respond to the ultraviolet light which accounts for ~5% of sunlight, however, visible light that accounts for ~50% of sunlight cannot be fully utilized[2]. In addition, these semiconductors have a high probability of recombination of photo-generated electrons and holes, resulting in the low utilization of photo-generated electrons. Moreover, the metals cannot be cathodically protected in dark condition. Therefore, it is necessary to develop a photocathode composite with low cost, visible light response, high electron utilization and electronstorage.

CdS with a direct band gap of 2.42 eV is a kind of important semiconductor which is currently considered as a significant material for scientific and technological applications[3-4]. At present, CdS is widely used in photocatalytic reduction of CO_2, photocatalytic hydrogen production and photocatalytic degradation[5-7]. Unfortunately, the ultrafast recombination of photo-generated charge carriers and the strong self-oxidation of CdS significantly restrict the practical applications in the photoelectrochemical field. The combination of CdS with another semiconductor is an efficient approach to improve the photocatalytic activity and stability[8]. Feng, *et al*[9]. reported that the formation of the CdS/Bi_2MoO_6 heterojunction contributed to the separation of photoinduced charge carriers. However, CdS has not been reported for photocathodic protection. Here, the combination of CeO_2 and CdS is examined for photoelectrochemical cathodic protection due to the suitable band gap (3.2 eV) of CeO_2. CeO_2 has been recently used as a photoactive material in solar cells and hydrogen evolution[10]. In addition, as reported, CeO_2 is used as an electron storage in photocathode protection because of the following conditions: (1) redox activity; (2) more posi-

Received date: 2019-01-28; **Modified date:** 2019-03-07
Foundation item: Fundamental Research Funds for the Central Universities (30916014103); Key R&D Programs of Jiangsu Province (BE2018649); Innovation Team of Six Talent Peaks of Jiangsu Province (XCL-CXTD-029); Key R&D Programs of Changzhou City (CE20185007)
Biography: WEI Ke-Nian (1978–), male, candidate of PhD. E-mail: kn@cczu.edu.cn
Corresponding authors: YAO Chao, professor. E-mail: yaochao420@163.com; Liu Xiao-Heng, professor. E-mail: xhliu@mail.njust.edu.cn

tive redox potential than the conduction band (CB) potential of the employed semiconductor; (3) more negative redox potential than the self-corrosion potential of the metal; (4) stability during repeated redox cycles[2,11].

Herein, CeO_2/CdS nanocomposites were prepared by a stepwise synthetic method to achieve a high photocathodic protection efficiency. CeO_2 nanoparticles were distributed on the surface of CdS sheets. The photocathodic protection properties of CeO_2/CdS including Tafel plots, the photo-induced current density, electrochemical impedance spectroscopy (EIS) and the photogenerated potential were investigated.

1 Experimental

1.1 Preparation of CdS nanosheets

Sulfur powder (0.374 g) and $CdCl_2·2.5H_2O$ (0.526 g) were dissolved in 70 mL diethylenetriamine (DETA) and stirred for 1 h. The mixed liquid was transferred to a Teflon liner and kept at a constant temperature of 80 ℃ for 24 h. Then, it was cooled to room temperature, centrifuged and washed with deionized water and ethanol. The product was dried at 60 ℃ for 12 h to obtain CdS nanosheets.

1.2 Preparation of CeO_2/CdS composites

Firstly, $Ce(NO_3)_3·6H_2O$ (0.76 g) was dissolved in 30 mL mixed solution consisted of water and ethylene glycol (mass ratio: 1/1), and stirred for 10 min. CdS (1.0 g) was added and stirred at 60 ℃. 25wt% ammonia solution (4.8 mL) was added in the mixture until the color of the mixed solution changed from dark green to yellow. Finally, the above mixture solution was centrifuged and washed with deionized water, then dried at 60 ℃ for 12 h to obtain 30wt% CeO_2/CdS whose ratio was 0.3∶1.0 For comparison, 10wt% CeO_2/CdS (0.1∶1.0) and 20wt% CeO_2/CdS (0.2∶1.0) composites were prepared by the similar method.

1.3 Characterization

The morphology was determined by JEOL-2100 transmission electron microscopy (TEM). X-ray diffraction (XRD) was recorded on a D/MAX 2500/PC powder diffractometer (Rigaku) applying Cu Kα radiation source from 5° to 80° (2θ) at a scanning rate of 3(°)/min. The UV-Vis diffuse reflectance spectra (DRS) were recorded on a UV-Vis spectrometer (Thermo Nicolet Evolution 500) equipped with an integrating sphere. The Photoluminescence (PL) spectra were carried on a fluorescence photometer (LS45) with the excitation wavelength of 300 nm.

1.4 Photoelectrochemical measurements

All electrochemical measurements were tested in a three-electrode experimental system at room temperature using CHI660D electrochemical workstation (Chenhua Instrument Co. Ltd, Shanghai, China). The experimental setup for photoelectrochemical protection measurements was shown in Fig.1.

The electrolyte was 3.5wt% NaCl aqueous solution. The prepared film photoanode served as the working electrode. Pt foil and a saturated calomel electrode (SCE) were used as the counter electrode and the reference electrode, respectively. The light source was a 300 W Xenon lamp in front of a quartz window incorporated into a conventional electrolytic cell. The working electrode was prepared as follows: the as-prepared samples were well dispersed in distilled water with proper content. The dispersion was uniformly dipped using a pipette gun (50 μL) on the surface of circle 304SS electrode. Simultaneously, Nafion solution was also coated on them until the dried composite film formed.

2 Results and discussion

Fig. 2 shows XRD patterns of CeO_2/CdS, pure CdS and CeO_2. The diffraction peaks at 2θ=26.5°, 28.2°, 43.7°, 47.8° and 51.8° are attributed to the (002), (101), (110), (103) and (112) planes of pure CdS (JCPDS 41-1049) respectively[6,12-13](Fig.2(a)).The peaks at 2θ=28.5°, 33.1°, 47.5° and 56.3° correspond to the (111), (200), (220) and (311) planes of pure CeO_2 (JCPDS 43-1002), respectively[12,14] (Fig. 2(e)). In Fig. 2(b–e), the peaks of CeO_2/CdS composites correspond to both CeO_2 and CdS with varying intensities, confirming the successful loading of CeO_2 nanoparticles on CdS nanosheets.

Fig.3 shows TEM images of different samples. CdS exhibits a sheet-like structure with a size of about 300 nm (Fig. 3(a)). A nanoparticle with a size of 3–5 nm

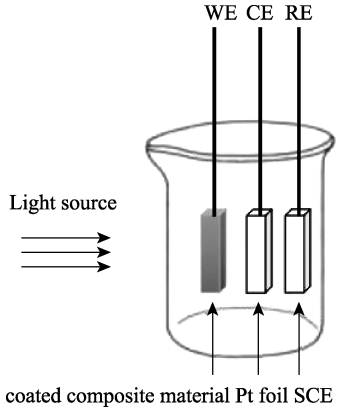

Fig. 1　Schematic sketch of the experimental setup for photoelectrochemical cathodic protection investigation

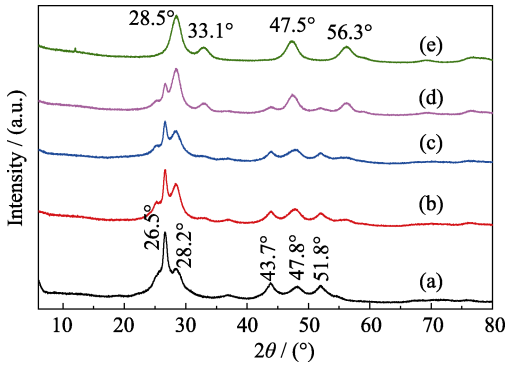

Fig. 2 XRD patterns of (a) CdS, (b) CeO_2/CdS (0.1 : 1.0), (c) CeO_2/CdS (0.2 : 1.0), (d) CeO_2/CdS (0.3 : 1.0) and (e) CeO_2

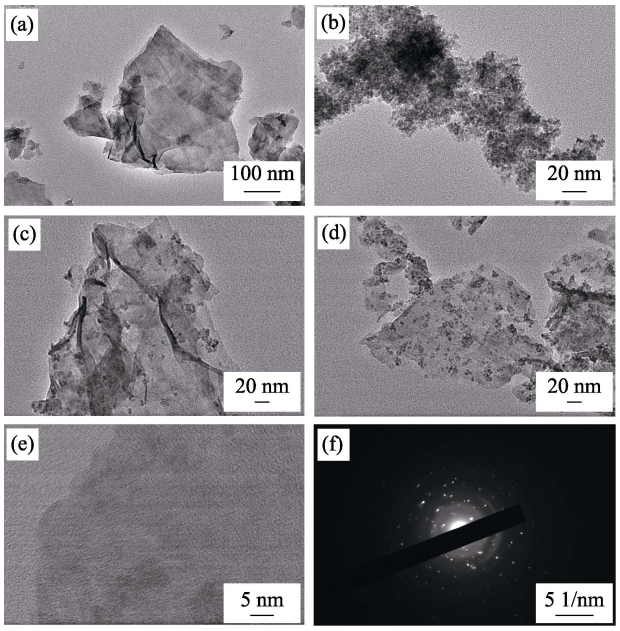

Fig. 3 TEM images of (a) CdS, (b) CeO_2, (c) CeO_2/CdS (0.1 : 1.0), (d) CeO_2/CdS (0.2 : 1.0), and (e) HRTEM image and EDX pattern of CeO_2/CdS (0.2 : 1.0)

can be observed (Fig. 3(b)). CeO_2 NPs are uniformly dispersed on CdS NSs with intimate interfacial contact which is beneficial to the efficient transfer of photogenerated charge (Fig. 3(c, d)). The HRTEM image confirms the formation of crystalline CeO_2 and CdS (Fig. 3(e)). The lattice spacing of 0.33 and 0.31 nm are assigned to (002) plane of CdS (JCPDS 41-1049) and (111) plane of CeO_2 (JCPDS 43-1002), respectively.

The light absorption of the samples are investigated by UV-Vis DRS (Fig. 4). Pure CeO_2 can absorb the visible light shorter than 460 nm while pure CdS can absorb the visible light shorter than 540 nm[6,12]. Compared with CdS and CeO_2, CeO_2/CdS composites exhibit an obvious red-shift in absorption edge while the absorption intensity in the range of 350–540 nm increases. This phenomenon is attributed to the formation of heterojunction between CdS and CeO_2 which reduces the recombination of electron-hole and enhances light absorption. Fig. 4(c)

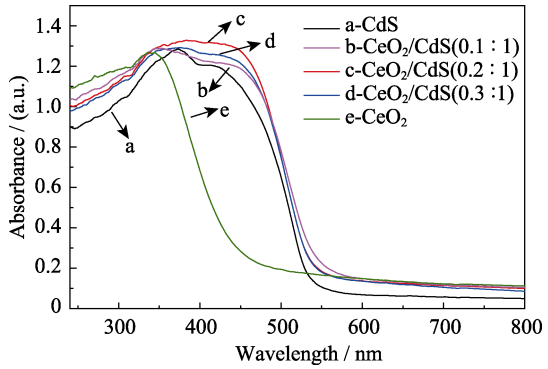

Fig. 4 UV-Vis diffuse reflection spectra of (a) CdS, (b) CeO_2/CdS (0.1 : 1.0), (c) CeO_2/CdS (0.2 : 1.0), (d) CeO_2/CdS (0.3 : 1.0) and (e) CeO_2

shows that CeO_2/CdS (0.2 : 1) has the highest absorption intensity (Fig. 4(c)).

Fig. 5 shows PL spectra of CdS, CeO_2/CdS with the different contents of CeO_2 (0.1wt%, 0.2wt%, and 0.3wt%). The lower the intensity, the lower the recombination rate is[15]. CdS presents the highest peak intensity, revealing the highest recombination rate. PL intensity of CdS is higher than that of CeO_2/CdS, implying the charge carrier recombination. CeO_2 nanoparticles are loaded on CdS nanosheets, which can efficiently separate the photogenerated charge carriers and inhibit the recombination of photogenerated charge carriers, leading to enhance photoelectrochemical cathodic protection. In particular, CeO_2/CdS (0.2 : 1.0) shows the lowest peak intensity, resulting in high photocatalytic activity.

Fig. 6 displays potentiodynamic polarization curves of 304SS coated with different materials in 3.5% NaCl under on–off response of white light irradiation. The corrosion potential of the uncoated 304SS is –192 mV (*vs.* SCE) corresponding to current density of about 1.15×10^{-5} mA·cm^{-2}. After coating, the corrosion potential of the coated 304SS in the dark becomes more positive, and the current density decreases by one order of magnitude, which can be ascribed to the barrier effect of the sheet-like CdS[16]. The 304SS coated with the

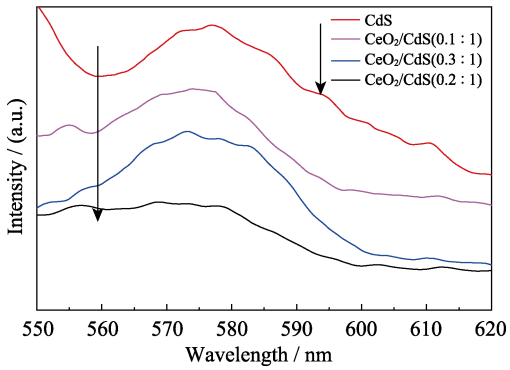

Fig. 5 PL spectra of CdS and CeO_2/CdS(0.1 : 1.0), CeO_2/CdS (0.2 : 1.0) and CeO_2/CdS(0.3 : 1.0)

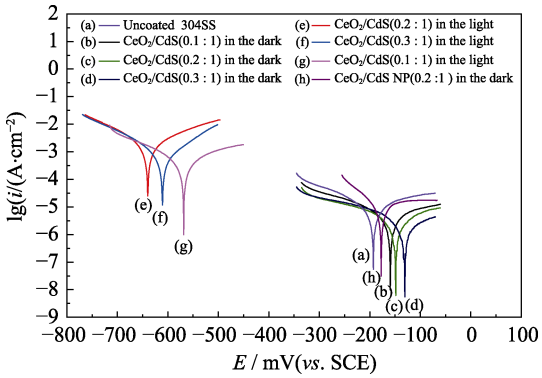

Fig. 6　(a–g) Polarization curves for uncoated 304SS, 304SS coated with CeO_2/CdS (0.1 : 1.0), CeO_2/CdS (0.2 : 1.0) and CeO_2/CdS (0.3 : 1.0) in the white-light illumination and in the dark; (h) polarization curves for CeO_2/CdS (0.2 : 1.0) nanoparticles in the dark

CeO_2/CdS (0.3 : 1.0) shows the highest potential (–129 mV) and the lowest current density (1.58×10^{-6} mA·cm^{-2}), which is related to the denser structure of CeO_2 nanoparticle and CdS nanosheets. Compared with bare 304SS, the corrosion potentials of 304SS coated with different composites are more negative and the current densities are higher under illumination, indicating that the composites generate photo-electrons and transfer to 304SS substrate[17]. Therefore, the 304SS substrate is under cathodic protection. The corrosion potential of the 304SS with CeO_2/CdS (0.2 : 1.0) coating is more negative (~–640 mV) and the photocurrent density is higher (~1.99×10^{-3} mA·cm^{-2}) under the light compared with the 304SS with CeO_2/CdS (0.1 : 1.0) coating and CeO_2/CdS (0.3 : 1.0) coating. It may be due to the formation of heterojunction between CeO_2 and CdS which reduces the recombination rate of electrons and holes, and transfer more electrons to the metal. For comparison, the corrosion potential of CeO_2/CdS (0.2 : 1.0) coating is more positive than that of CeO_2/CdS (0.2 : 1.0) nanoparticles, suggesting that flake-like CdS possesses excellent physical barrier.

The transient photo-current responses of the coatings were observed upon on/off cycles of intermittent visible light illumination in Fig. 7. All the samples exhibit fast reproducible photoresponse under visible light illumination. Obviously, the current density rises sharply when the light is turned on. The current density rapidly decays to almost zero when the light is turned off. The photocurrent density of the composites is higher than that of pure CdS, which is attributed to the formation of heterojunction between CeO_2 and CdS. Under light illumination, the electrons in the CB of CdS can be more easily transferred to more positive CB of CeO_2, which leads to the higher photocurrent of the composites[18]. The photocurrent density of CeO_2/CdS (0.2 : 1.0) is the highest (~700 μA/cm^2) which is consistent with the potentiodynamic polarization curves in Fig. 5. Moreover, no noticeable photocurrent degradation is detected after several on/off cycles of light illumination, indicating that the prepared films possess good photostability.

In order to evaluate the photoelectron separation, transport efficiency and corrosion resistance of the composites, EIS was tested (Fig. 8). In this model, C_f and R_f at high frequencies represent the capacitance and resistance of the coating while C_{dl}, R_{ct} and R_s at low frequencies represent the double-layer capacitance, charge transfer resistance and electrolyte resistance, respectively[18]. Table 1 shows the fitting results of EIS spectra with

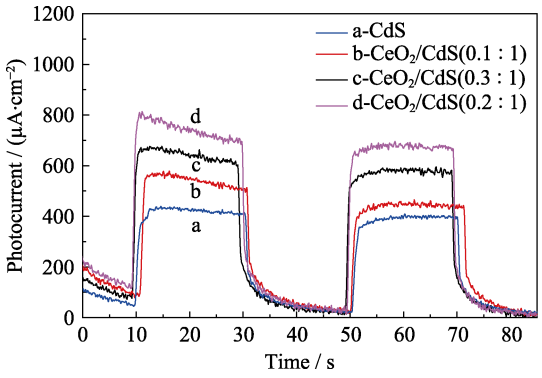

Fig. 7　Photocurrent-time curves of (a) CdS, (b) CeO_2/CdS (0.1 : 1.0), (c) CeO_2/CdS (0.3 : 1.0) and (d) CeO_2/CdS (0.2 : 1.0)

Table 1　Fitting results of the Nyquist plots using the equivalent circuits of Fig. 8

Electrode	R_s /Ω	Q_f		R_f/Ω	Q_{dl}		R_{ct}/Ω
		Y_0	n		Y_0	n	
CeO_2/CdS(0.3 : 1.0)[a]	5.548	3.32×10^{-5}	0.914	1.35×10^{6}	5.11×10^{-5}	1.000	3.73×10^{5}
CeO_2/CdS(0.2 : 1.0)[a]	4.889	2.85×10^{-5}	0.917	3.35×10^{5}	5.02×10^{-5}	1.000	2.30×10^{5}
CeO_2/CdS(0.1 : 1.0)[a]	4.615	1.97×10^{-5}	0.945	1.34×10^{5}	5.62×10^{-5}	0.907	2.15×10^{5}
CdS[a]	4.041	2.22×10^{-4}	0.987	1.30×10^{5}	2.46×10^{-5}	0.949	2.40×10^{5}
uncoated 304SS	4.413	5.99×10^{-5}	1.000	4.50×10^{4}	6.27×10^{-5}	0.903	2.70×10^{5}
CdS[b]	1.968	1.79×10^{-4}	1.000	8.10×10^{3}	4.12×10^{-4}	0.843	2.19×10^{4}
CeO_2/CdS(0.1 : 1.0)[b]	3.928	1.10×10^{-3}	0.766	1.43×10^{4}	5.56×10^{-5}	0.884	1.58×10^{4}
CeO_2/CdS(0.2 : 1.0)[b]	13.39	9.21×10^{-6}	0.859	2.36×10^{3}	1.07×10^{-6}	0.914	1.15×10^{3}
CeO_2/CdS(0.3 : 1.0)[b]	4.021	3.47×10^{-3}	0.533	3.14×10^{4}	8.46×10^{-5}	0.903	4.35×10^{3}

a-In dark condition; b-Under light illumination

different coated electrodes in 0.5 mol/L H_2SO_4 solution with and without visible light irradiation.

In Fig. 8(a), CeO_2/CdS presents an excellent corrosion resistance in the dark because the resistance of CeO_2/CdS coating is much larger than that of bare 304SS electrode[16]. From the fitting results in Table 1, the R_f value of CdS nanosheets ($1.30\times10^5\ \Omega$) is one order of magnitude higher than that of bare 304SS electrodes ($4.50\times10^4\ \Omega$). The sheet material shields the penetration of corrosion factors such as water, oxygen and ions, and the overlapping flakes that are parallel to each other can prolong the path of corrosion factor penetration, thus improving the corrosion resistance of the 304SS. With the increasing content of CeO_2, the R_f of the composite coatings becomes larger. The R_f of CeO_2/CdS (0.3 : 1.0) coating ($1.35\times10^6\ \Omega$) is one order of magnitude higher than that of CdS nanosheet ($1.30\times10^5\ \Omega$), which is the result of the dense structure of CeO_2 nanoparticles and overlapping CdS nanosheets.

The arc diameter of the 304SS electrode with composite coatings is significantly smaller than that of the bare 304SS electrode under light irradiation (Fig. 8(a)). The charge transfer resistance (R_{ct}) decreases significantly (Table 1), which is consistent with the trend of the Tafel polarization curve. These photoelectrons can reach 304SS and lead to the negative shift of the corrosion potential. In this process, the heterojunction between CeO_2 and CdS promotes the separation and transport of electrons and holes[19]. The charge-transfer resistance ($1.15\times10^3\ \Omega$) of CeO_2/CdS (0.2 : 1.0) is the smallest in the composites, which is two orders of magnitude lower than that of bare 304SS electrode ($2.70\times10^5\ \Omega$). Therefore, CeO_2/CdS (0.2 : 1.0) composite under light irradiation has the highest charge separation and transfer efficiency.

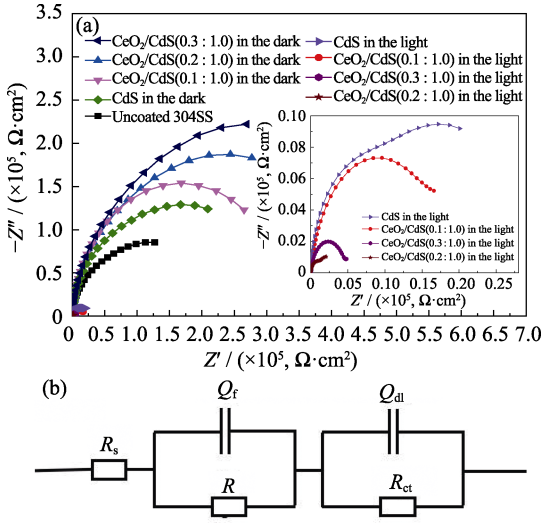

Fig. 8 (a) Nyquist plots of pure 304SS, 304SS coupled with CdS and CeO_2/CdS(0.1 : 1), CeO_2/CdS(0.2 : 1) and CeO_2/CdS (0.3 : 1) in the dark and white-light illumination; (b) Schematics of the equivalent circuit obtained by EIS result fitting

Fig. 9 shows the open circuit potential (OCP) curves for 304SS in 3.5wt% NaCl solution under the visible light irradiation. The uncoated 304SS electrode potential is –189 mV (Fig. 9(a)). In the dark, 304SS electrode with CdS nanosheet coating and CeO_2/CdS (0.2 : 1.0) coating are –160 mV (SCE) and –130 mV (SCE), respectively, which are consistent with the results of Fig. 6. The sheet-like structure of CdS plays a good barrier, indicating that the composites can be used as a protective layer on the substrate[17,19].

When the light is turned on, the potential of the 304SS electrode drops sharply and stays at a more negative potential due to the generation of photo-generated electrons. The potential of the 304SS electrode rises when the light is turned off[19-20]. Consistent with the results of Fig. 6 and Fig. 7, potential of the 304SS with CeO_2/CdS (0.2 : 1.0) coating electrode (–632 mV (SCE)) is more negative than that of CdS coating (–510 mV (SCE)), due to the formation of a heterojunction between CdS and CeO_2. The potential of 304 SS electrode with CdS coating rapidly rises back to the initial potential value while the potential 304 SS electrode with CeO_2/CdS (0.2 : 1.0) coating slowly rises and remains at a lower potential when the light is turned off, which can be attributed to the storage electron function of ceria[19-20]. The coupled semiconductor CeO_2 is capable of storing the excess electrons which can be released during the dark. The cathodic protection can still continue before illumination is restored. Fig. 9(b) shows that CeO_2/CdS (0.2 : 1.0) composites can provide electrons for 304SS in the dark for up to 12 h.

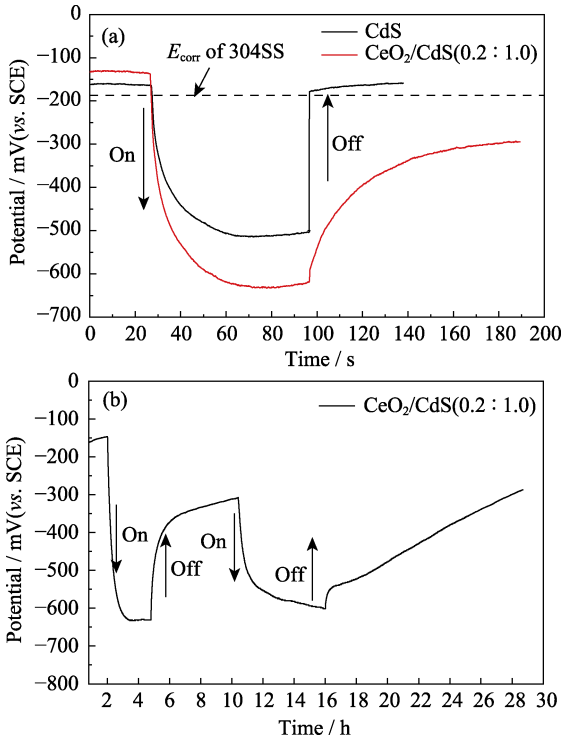

Fig. 9 OCP variations of 304SS electrodes coupled with the as-obtained samples

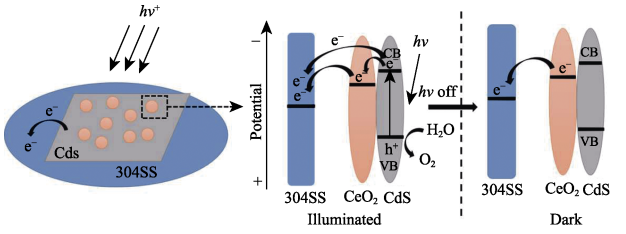

Fig. 10　Mechanism of CeO_2/CdS composite for 304SS photocathodic protection

Based on the above results and discussion, the possible photocathodic protection mechanism of CeO_2/CdS composite for 304SS is proposed in Fig. 10. Photogenerated electrons on the CB of CdS can easily be transferred to 304SS under light irradiation, because the conductive potential of CdS is more negative than the self-corrosion potential of 304SS[21]. Some photogenerated electrons of CdS is conducted to CeO_2 attributed to the conductive potential of CdS which is more negative than the redox potential of CeO_2[11]. CeO_2 achieves the storage and release of electrons through the following redox reactions:

$$CeO_2 + xe^- + xM^+ \rightarrow M_xCeO_2 \qquad (1)$$

where M=H and x=1[11,21]. When the light is turned off, the electrons stored in CeO_2 are released and transferred to the 304SS to maintain the cathodic protection effect. Therefore, 304SS can be protected even in the dark. In summary, CeO_2/CdS composite can provide an enduring protection for 304SS.

3　Conclusion

CeO_2/CdS composites were fabricated by a stepwise synthetic approach. Under the light illumination, CeO_2/CdS exhibits an enhanced photo-induced current density and a more negative photo-potential shift as compared with pure CeO_2 and pure CdS due to the formation of a heterojunction between them, which reduces the recombination of electron-hole pairs and improves the efficiency of photo-electric conversion. Furthermore, CeO_2/CdS can continue to provide cathodic protection in the dark because CeO_2 has the function of storing electrons. At last, flake-like CdS can slow down the penetration of corrosion factors and act as a physical barrier. A variety of mechanism work synergistically to make CeO_2/CdS nanocomposites have a more effective photo cathodic protection on 304SS.

References:

[1] XU H M, LIU W, CAO L X, *et al*. Preparation of porous TiO_2/ZnO composite film and its photocathodic protection properties for 304 stainless steel. *Appl. Surf. Sci.*, 2014, **301(10):** 508–514.

[2] BU Y, AO J P. A review on photoelectrochemical cathodic protection semiconductor thin films for metals. *Green Energy & Environ.*, 2017, **2(4):** 331–362.

[3] LI Q, LI X, WAGEH S, *et al*. CdS/graphene nanocomposite photocatalysts. *Advanced Energy Materials*, 2015, **5(14):** 1–28.

[4] FU X L, WU Z P, LEI M, *et al*. A facile route to silver–cadmium sulfide core-shell nanoparticles and their nonlinear optical properties. *Mate. Lett.*, 2013, **104(3):** 76–79.

[5] IJAZ S, EHSAN M F, ASHIQ M N, *et al*. Preparation of CdS@CeO_2 core/shell composite for photocatalytic reduction of CO_2 under visible-light irradiation. *Appl. Surf. Sci.*, 2016, **390:** 550–559.

[6] MA S, XIE J, WEN J Q, *et al*. Constructing 2D layered hybrid CdS nanosheets/MoS_2 heterojunctions for enhanced visible-light photocatalytic H_2 generation. *Appl. Surf. Sci.*, 2017, **391:** 580–591.

[7] YAO L L, GU J J, WANG W Q, *et al*. Ce^{4+} as a facile and versatile surface modification reagent for templated synthesis in electrical applications. *Nanoscale*, 2019, **11:** 2138–2142.

[8] YU J G, JIN J, CHENG B, *et al*. A noble metal-free reduced graphene oxide-CdS nanorod composite for the enhanced visible-light photocatalytic reduction of CO_2 to solar fuel. *J. Mater. Chem. A*, 2014, **2(10):** 3407–3416.

[9] FENG Y, YAN X, LIU C B, *et al*. Hydrothermal synthesis of CdS/Bi_2MoO_6 heterojunction photocatalysts with excellent visible-light-driven photocatalytic performance. *Appl. Surf. Sci.*, 2015, **353:** 87–94.

[10] CHAUDHARY Y S, PANIGRAHI S, NAYAK S, *et al*. Facile synthesis of ultra-small monodisperse ceria nanocrystals at room temperature and their catalytic activity under visible light. *J. Mater. Chem.*, 2010, **20(12):** 2381–2385.

[11] SUBASRI R, DESHPANDE S, SEAL S, *et al*. Evaluation of the performance of TiO–CeO bilayer coatings as photoanodes for corrosion protection of copper. *Electrochem. Solid S L*, 2006, **9(1):** B1–B4.

[12] ZHANG P, LIU Y, TIAN B Z, *et al*. Synthesis of core-shell structured CdS@CeO_2 and CdS@TiO_2 composites and comparison of their photocatalytic activities for the selective oxidation of benzyl alcohol to benzaldehyde. *Cataly. Today*, 2017, **281:** 181–188.

[13] FANG J, XU L, ZHANG Z Y, *et al*. Au@TiO_2-CdS ternary nanostructures for efficient visible-light-driven hydrogen generation. *ACS Appl. Mater. Inter.*, 2013, **5(16):** 8088–8092.

[14] PAL P, SINGHA R K, SAHA A, *et al*. Defect-induced efficient partial oxidation of methane over nonstoichiometric Ni/CeO_2 nanocrystals. *J. Phys. Chem. C*, 2015, **119(24):** 13610–13618.

[15] ZHAO H X, CUI S, YANG L, *et al*. Synthesis of hierarchically meso-macroporous TiO_2/CdS heterojunction photocatalysts with excellent visible-light photocatalytic activity. *J. Colloid Interf. Sci*, 2018, **512:** 47–54.

[16] GUO X Q, LIU W, CAO L X, *et al*. Graphene incorporated nanocrystalline TiO_2 films for the photocathodic protection of 304 stainless steel. *Appl. Surf. Sci.*, 2013, **283(11):** 498–504.

[17] ZHANG T T, LIU Y, LIANG J, *et al*. Enhancement of photoelectrochemical and photocathodic protection properties of TiO_2 nanotube arrays by simple surface UV treatment. *Appl. Surf. Sci.*, 2017, **394:** 440–445.

[18] HU J, GUAN Z C, LIANG Y, *et al*. Bi_2S_3 modified single crystalline rutile TiO_2 nanorod array films for photoelectrochemical cathodic protection. *Corros. Sci.*, 2017, **125:** 59–67.

[19] REN J F, QIAN B, LI J, *et al*. Highly efficient polypyrrole sensitized TiO_2 nanotube films for photocathodic protection of Q235 carbon steel. *Corros. Sci.*, 2016, **111:** 596–601.

[20] HU J, LIU Q, ZHANG H, *et al*. Facile ultrasonic deposition of SnO_2 nanoparticles on TiO_2 nanotube films for enhanced photoelectrochemical performances. *J. Mater. Chem. A*, 2015, **3(45):** 22605–22613.

[21] TATSUMA T, SAITOH S, OHKO Y, *et al*. TiO_2-WO_3 photoelectrochemical anticorrosion system with an energy storage ability. *Chem. Mater.*, 2001, **13(9):** 2838–2842.

高性能 CeO_2/片状 CdS 复合光电极材料的制备及在光阴极保护中应用

魏科年[1,2], 刘 展[2], 左士祥[2], 严向玉[2], 吴凤芹[2],
李霞章[2], 姚 超[1,2], 刘孝恒[1]

(1. 南京理工大学 软化学与功能材料教育部重点实验室, 南京 210094; 2. 常州大学 石油化工学院, 江苏省先进催化与绿色制造协同创新中心, 常州 213164)

摘 要: 通过逐步合成法制备了具有储存电子和物理阻隔功能的 CeO_2/CdS 纳米复合材料, 并用于光电阴极保护。通过 XRD, TEM, UV-Vis 和 PL 等手段对制备的纳米复合材料进行表征。在模拟白光照射下研究不同质量比的 CeO_2/CdS 复合材料的光电化学性质。在黑暗条件下, 涂有 CeO_2/CdS(质量比 0.2∶1.0)的 304 不锈钢涂层的电位比 CeO_2/CdS(质量比 0.2∶1.0)粒子涂层更正。在白光照射下, CeO_2/CdS(质量比 0.2∶1.0)复合材料的最大光电流密度为 700 μA·cm^{-2}, 涂有 CeO_2/CdS(质量比 0.2∶1.0)的 304 不锈钢涂层的电位为–650 mV(*vs.* SCE), 明显低于 304 不锈钢腐蚀电位(–200 mV *vs.* SCE), 表明片状 CdS 具有物理阻隔性能及 CeO_2/CdS 复合材料具有显著的光电化学性能。这主要是由于 CeO_2 纳米颗粒和 CdS 纳米片之间形成了异质结, 促进了光致电子和空穴的有效分离, 从而提高了光电转换效率。此外, 由于 CeO_2 具有储存电子的功能, 在黑暗条件下可以继续释放电子, 能够提供 12 h 的阴极保护性能。

关 键 词: CeO_2/CdS 复合材料; 异质结构; 物理阻隔; 光电化学阴极保护

中图分类号: TB332 **文献标识码:** A